

Many-body localization and mobility edge in a disordered Heisenberg spin ladder

Elliott Baygan, S. P. Lim and D.N. Sheng

Department of Physics and Astronomy, California State University, Northridge, California 91330, USA

We examine the interplay of interaction and disorder for a Heisenberg spin ladder system with random fields. We identify many-body localized states based on the entanglement entropy scaling, where delocalized and localized states have volume and area laws, respectively. We first establish the quantum phase transition at a critical random field strength $h_c \sim 8.5 \pm 0.5$, where all energy eigenstates are localized beyond that value. Interestingly, the entanglement entropy and fluctuation of the bipartite magnetization show distinct probability distributions which characterize different quantum phases. Furthermore, we show that for weaker h , energy eigenstates with higher energy density are delocalized while states at lower energy density are localized. This defines a mobility edge and a mobility gap separating these two phases. By following the evolution of low energy eigenstates, we observe that the mobility gap grows with increasing the random field strength, which drives the system to the phase of the full many-body localization with increasing disorder strength.

PACS numbers: 75.10.Pq, 71.30.+h, 73.22.Gk

I. INTRODUCTION

Anderson localization theory¹ predicts that noninteracting electrons are generally localized in one and two-dimensional (1D and 2D) disordered systems without either a magnetic field or spin-orbit coupling due to destructive quantum interference. It is generally believed that low energy states remain localized for weakly interacting systems²⁻⁷ with characteristic features different from noninteracting systems. Recently, there is renewed interest to examine the Anderson localization for interacting systems, where the phenomenon of many-body localization (MBL)^{8,9} has attracted intense studies. Many remarkable properties of an MBL phase has been established⁸⁻⁴⁶ based on combined theoretical and numerical studies. For disordered interacting systems, the random disorder can drive a dynamic quantum phase transition^{8,22,47} from a delocalized state to an MBL phase, where energy eigenstates at finite energy density become localized. From the quantum information perspective, energy eigenstates in an MBL phase have suppressed entanglement entropy satisfying an area law^{8,17,26,36} scaling with the subsystems boundary area in contrast to the volume law scaling expected for an ergodic delocalized state. As a consequence, the MBL phase is non-ergodic and can not thermalize^{11,48,49}, which also challenges the fundamental “eigenstate thermalization hypothesis” (ETH) for quantum statistical physics⁵⁰. The MBL state may exhibit quantum order or topological order^{16,36,43,51-55} at finite temperature as excitations at finite energy density are localized. A phenomenological study¹⁴ further establishes that the MBL phase behaves like integrable systems, respecting extensive numbers of local conservation laws^{15,20,56}. The quantum phase transition from an MBL phase to a delocalized ergodic phase may be continuous characterized by a jump of the entanglement entropy in the thermodynamic limit¹⁷, where both entropy and its variance grow with the system volume at the critical point^{14,26}. Interestingly, it is conjectured that an MBL phase can also have a continuous localization-delocalization transition to a new state, where the delocalized phase is non-ergodic whose volume law entanglement entropy tends to zero as the transition is approached¹⁷. It may be possi-

ble to have the MBL phase in multi-component systems without random disorder^{57,58}. The MBL phase may be detected experimentally in cold atom systems^{12,13,18,19}.

So far, much of the quantitative understanding of MBL systems are based on numerical exact diagonalization (ED) studies^{12,19,21-36,59} of spin and electron systems, where the dynamic quantum phase transition between a delocalization phase to an MBL phase has been demonstrated for different 1D model systems with spin (or particles) numbers in the range of $N = 10 - 22$ ^{26,46}. There are also some recent developments⁶⁰⁻⁶⁵ using tensor network and density matrix renormalization group approaches to study such systems. One of the conceptually important and unsettled issue is if the mobility edge exists for microscopic system to separate the low energy localized state from the higher energy extended states. On the one hand, these ED studies^{26,46} have demonstrated the energy density dependence of the critical random field, consistent with the existence of the mobility edge. In particular, Luitz et al.⁴⁶ studied the 1D Heisenberg chain in a random field using the shift-inverted spectral transformation method dealing with up to 22 spins, where the finite-size scaling has been demonstrated with convincing accuracy supporting the existence of the mobility edge. However, the recent numerical linked cluster expansion study⁶⁶ for a thermodynamic system finds that a higher disorder strength (as the lower bound) is required to enter the MBL phase than that obtained by ED studies. The reason for such a discrepancy remains not understood. On the theoretical side, it is not clear^{32,44,67-69} if some spatial region with higher energy density may play an important role with more extensive wavefunctions, which may melt the lower energy eigenstates in the system into delocalized states with increasing the system size. Some insight on this issue may come from the earlier study of interacting many-body systems with random disorder^{70,71}, which exhibit the fractionalized quantum Hall effect. In such a system, we have demonstrated that low energy states below a mobility edge have topological order protected by a mobility gap which separates the low energy localized insulating states from the metallic states above the mobility gap. These earlier studies suggest that it is possible to follow the evolution of the low energy eigenstates in disordered interacting systems to detect if the mobility gap

generally exists for MBL systems.

In this paper, we numerically examine the interplay of interaction and random disorder field for two-leg Heisenberg ladder systems, which stands between 1D and 2D systems⁴⁰, with the latter being much harder to be systematically studied based on ED method. We identify MBL states based on the bipartite entanglement entropy scaling, and the spectral statistics of many-body energy levels. We first establish the quantum phase transition at a critical random field strength $h_c \sim 8.5 \pm 0.5$, where all energy eigenstates are localized beyond that value. Interestingly, the entanglement entropy shows distinct probability distribution in different quantum phases, while transition is associated with the divergent variance for the entropy at the thermodynamic limit^{26,46}. Despite the small system sizes we can access with the number of spins $N = 12 - 20$, our entropy distribution matches to the theoretic prediction⁶⁷ in both delocalized Griffiths phase and MBL phase indicating we were able to access universal characteristics of these different quantum phases. Furthermore, we show that at weaker h , energy eigenstates with higher energy density are delocalized while states at lower density are localized, which defines a mobility edge separating these two dynamically distinct quantum phases in agreement with earlier results for 1D spin chain systems^{26,46}. The associated mobility gap (the excitation gap of the lowest energy extended state to groundstate) may be relevant for experimental measurement as it plays the role of the activation gap^{70,72} for quantum transport. By following the evolution of low energy eigenstates, we observe that the mobility edge moves to higher energy density with the increase of the random field strength, which eventually drives the system to the phase with full MBL where all energy eigenstates are localized. The remaining of the paper is organized as following: In Sec. II, we first introduce the two-leg ladder spin model with random fields and briefly discuss the method we use to study the system. We present the evidence of the MBL phase determined by the entanglement entropy and the energy level statistics studies. In Sec. III, we study the characteristic features of the quantum phases and the transition between the delocalized phase and the MBL phase. We also present the evidence for the mobility edge separating the low energy localized phase from the higher energy extended states. Finally, in Sec. IV, we summarize our main results and discuss open questions.

II. SPIN MODEL AND TRANSITION TO AN MBL PHASE

We study the Heisenberg two leg ladder spin system on the square lattice with the following Hamiltonian:

$$H = J \sum_{\langle i,j \rangle} \vec{S}_i \cdot \vec{S}_j - \sum_i h_i S_i^z,$$

where the summation $\langle i,j \rangle$ runs over all distinct nearest neighbor bonds with antiferromagnetic coupling J , which is set as the units of the energy $J = 1$. The h_i is a random magnetic field coupling, which distributes uniformly between window $(-h, h)$ with h as the strength of random fields.

The number of sites of the ladder system can be written as $N = N_x N_y$ with $N_y = 2$ and N_x is the number of sites along each spin chain.

We perform Lanczos ED calculations to obtain energy eigenstates around a fixed value E determined by the target energy density ε for systems with the number of sites $N = 12 - 20$ in the total $S_z = 0$ sector. Specifically, for each disorder configuration, we first calculate the ground state energy E_0 and the maximum energy E_{\max} , which are used to define the target energy density $\varepsilon = (E - E_0)/(E_{\max} - E_0)$. We perform more than 1000 disorder configuration average for most systems we studied. Physical quantities⁴⁶ including the bipartite entanglement entropy, energy level statistics and bipartite fluctuation of the subsystem magnetization are obtained and averaged over disorder configurations and sometimes also averaged over 30 energy eigenstates with energies

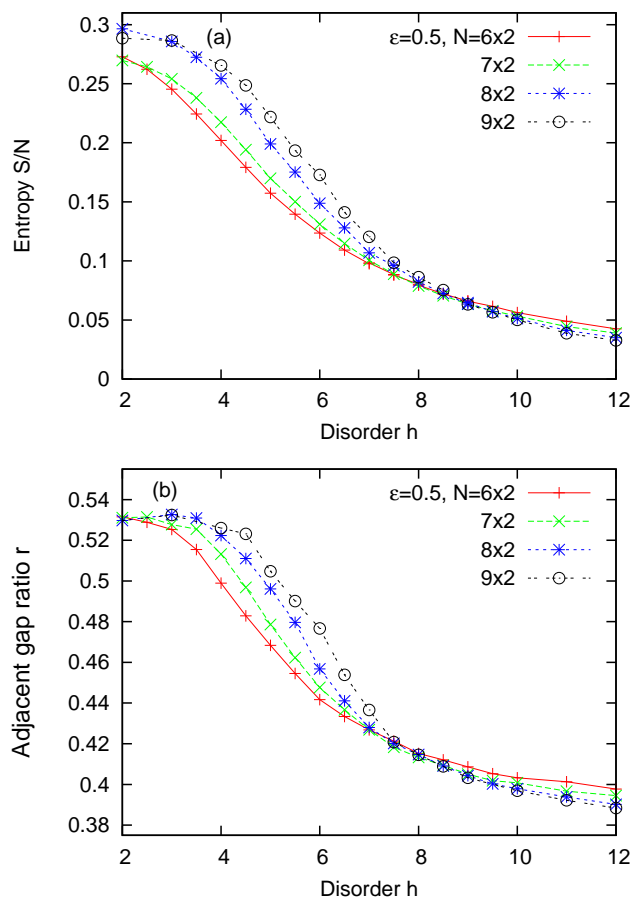


FIG. 1: (Color online) (a) The ratio of entanglement entropy over the number of system sites S/N for different systems from $N = 6 \times 2$ to 9×2 at the energy density $\varepsilon = 0.5$ as a function of random disorder strength h . Curves for different N approximately cross each other around a critical random field strength $h_c = 8.5 \pm 0.5$. (b) The adjacent gap ratio r for states with energy density $\varepsilon = 0.5$ as a function of disorder strength h . Here we see that on small h side, r approaches the Gaussian orthogonal ensemble value (0.5307) representing delocalized states, while at larger h side, r reaches the Poisson value ($2 \ln 2 - 1 \simeq 0.3863$) for larger systems representing localized states. All curves cross around the critical value $h_c = 8.0 \pm 0.7$.

closest to the given energy density ε as detailed below.

The bipartite entanglement entropy has been extensively used as an effective tool to characterize quantum phases for such an interacting system^{8,26,46}. We compute the Von Neumann entanglement entropy of the ladder system from all eigenvalues of the reduced density matrix ρ_A as $S = -\text{Tr}\rho_A \ln \rho_A$, by partitioning the system in the middle along the vertical direction (the lengths for two subsystems A and B are the integer-parts of $N_x/2$ and $(N_x + 1)/2$, respectively). For an interacting system with weak disorder, the entanglement entropies of higher energy eigenstates are expected to follow the volume law and these states are ergodic satisfying the ETH^{8,9}. This is in contrast to the behavior of the ground state, where the entanglement entropy follows the area law (with possibly up to the logarithmic correction depending on if there are gapless excitations)¹⁷. By varying the disorder strength h , one can detect the possible quantum phase transi-

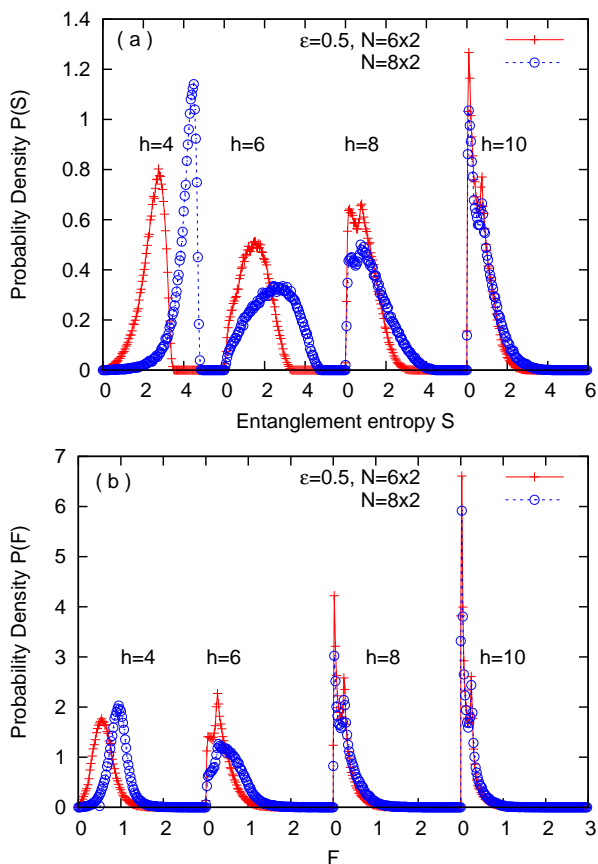


FIG. 2: (Color online) (a) The probability distributions of the bipartition entanglement entropy $P(S)$ for spin system at energy density $\varepsilon = 0.5$ with different disorder strengths $h = 4, 6, 8$ and 10 for system sizes $N = 6 \times 2$ and 8×2 . These results illustrate that for stronger disorder case, the distribution always has a long tail into higher S values, while for smaller h the long tail is on small S side. (b) The probability distributions $P(F)$ of the variance $F = \langle (S_A^z)^2 \rangle - \langle S_A^z \rangle^2$ (in units of the square of the Planck constant \hbar^2) of the magnetization of the half system A for spin system at energy density $\varepsilon = 0.5$ with different disorder strengths $h = 4, 6, 8$ and 10 for $N = 6 \times 2$ and (b) 8×2 .

tion from the behavior of the entanglement entropy^{26,46}. As shown in Fig. 1(a), we plot the ratio of entanglement entropy over the number of system sites S/N for different systems from $N_x = 6$ to 9 at the energy density $\varepsilon = 0.5$ as a function of random field strength h . On the smaller h side, we see the ratio S/N increases with system sizes N and approaches a constant indicating the volume law growth of S . With varying h , all data points approximately cross each other around a critical value $h_c \sim 8.5 \pm 0.5$. On the larger h side, S/N approaches zero indicating the low entanglement and non-ergodic behavior where energy eigenstates are localized. The ladder systems we study here have stronger finite size effect (from the even-odd effect of N_x) than the 1D spin chain systems, which is the reason that not all curves cross at the same point in Fig. 1(a).

We further use the level statistics analysis from the random matrix theory^{21,73} to probe the localization-delocalization characteristics of energy eigenstates. In the delocalized regime, the level-spacing distribution is described by the Gaussian orthogonal ensemble (GOE) statistics, which represents extended levels with level-repulsion between them because of the overlap of energy eigenstates in real space. In the localized regime, the level-spacing distribution is determined by Poisson statistics as wave-functions close in energy are exponentially localized with no level repulsion between them⁷⁴. In the energy spectrum analysis⁴⁶, we define the energy gap $\delta_n = E_n - E_{n-1}$ as the energy difference between the n -th and $(n-1)$ -th eigenstates, then the adjacent gap ratio can be defined as $r_n = \min(\delta_n, \delta_{n+1}) / \max(\delta_n, \delta_{n+1})$. We average the gap ratio $r = \langle r_n \rangle$ over states near the spectrum center at $\varepsilon = 0.5$ for 30 eigenstates and 1000 random disorder configurations for each given disorder strength h . As shown in Fig. 1(b), we see that at the small h side, r approaches the Gaussian orthogonal ensemble value (0.5307) representing delocalized states, while at stronger h side, r reaches the Poisson value ($2 \ln 2 - 1 \simeq 0.3863$) for larger systems rep-

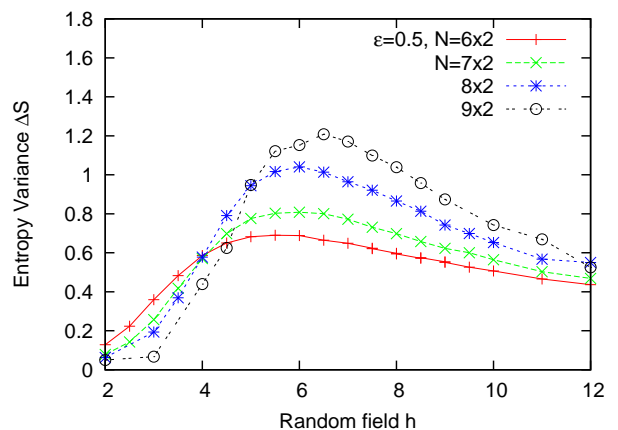


FIG. 3: (Color online) (a) The variance $(\Delta S)^2 = \langle S^2 \rangle - \langle S \rangle^2$ of the entanglement entropy at energy density $\varepsilon = 0.5$ for different h . ΔS reaches the peak value at h_p smaller than the identified h_c for quantum phase transition. Clearly, h_p shifts to higher h with the increase of N .

representing the level statistics of localized states. All curves cross around the critical value $h_c \sim 8.0 - 8.5$. Due to the stronger finite size effect coming from the even-odd effect for N_x , we are not attempting to do a finite-size scaling. Instead, we will focus on the universal behavior of the different phases to explore the nature of the quantum phases and the transition involved here.

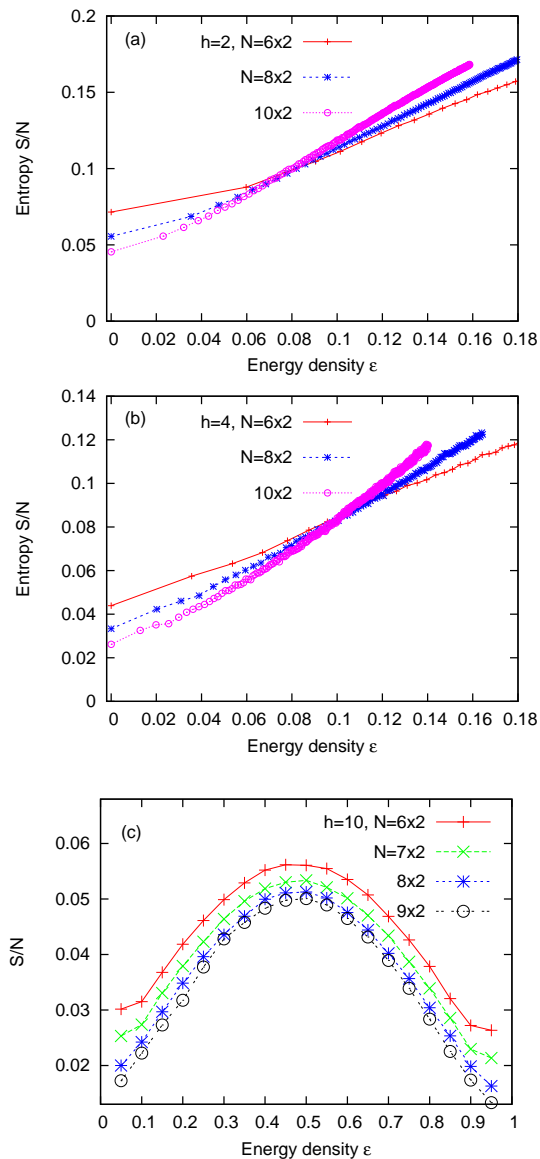


FIG. 4: (Color online) The entropy of each energy eigenstate S_i for low energy eigenstates averaged over disorder configurations is shown as a function of its average energy density. S_i/N curves for different system sizes $N = 6 \times 2, 8 \times 2$ and 10×2 cross at a critical energy density ε_c , which separates the higher energy delocalized states from the lower energy localized states.

III. NATURE OF QUANTUM PHASES AND PHASE TRANSITION

A. Probability distributions of entanglement entropy and variance of bipartite magnetization

Now we turn to the study of the probability distribution of the entropy $P(S)$ for spin system at energy density $\varepsilon = 0.5$ for different disorder strengths $h = 4, 6, 8$ and 10 crossing two different phases obtained for ensembles with 30 energy eigenstates and 1000 disorder configurations for each h . As shown in the Fig. 2(a), on the small h side, we see that the peak position of the distribution $P(S)$ (which reflects the average of S) moves to the larger S value with increasing system size N , indicating a consistency with the volume law for the entropy. Close to the transition point for $h = 6$ we find that the distribution $P(S)$ becomes much broadened while the peak position moves to the higher S with the increase of N , but the peak height reduces at the same time. As we move to the higher h side, we see that the distribution again becomes sharper, with two peaks showing for each $P(S)$ curve which may be related to the non-ergodic character of the localized phase. Furthermore, we also see that for the stronger disorder case, the distribution always has a long tail into higher S values, while for smaller h the long tail is at the smaller S side. To compare with recent theoretical description of the MBL of 1D system⁶⁷, we find that the entropy distribution is very similar to the ones obtained based on their real space renormalization group simulations. Specifically, at $h = 4$ our distribution has a long tail in small S region, which matches to the one for the Griffiths phase just before the transition to the MBL phase. At $h = 10$, we find the $P(S)$ is peaked at $S = 0$ and shows an exponential decay tail on the larger S side.

We compare the entanglement entropy behavior with the bipartite fluctuations F of the subsystem magnetization S_A^z ^{46,75}, which is defined as $F = \langle (S_A^z)^2 \rangle - \langle S_A^z \rangle^2$ as shown in Fig. 2(b). The distribution $P(F)$ exhibits very similar behavior as $P(S)$ for h closer to the quantum phase transition and in the MBL phase. The similar two-peaks structure is also clear for $P(F)$ on the larger h side in the MBL phase. The only difference worth mentioning is that with weaker disorder $h = 4$, the $P(F)$ demonstrates the normal Gaussian distribution, which is sharp and near symmetric about the peak.

The variance of the entanglement entropy has been shown to be an excellent quantity^{26,67} for identifying the quantum phase transition from 1D spin chain studies. Here we show the variance ΔS of the entanglement entropy averaged over 30 different energy eigenstates around the energy density $\varepsilon = 0.5$ and 1000 disorder configurations. In agreement with these observations for 1D systems^{26,46}, we find that the ΔS is small in both small h and large h sides, and demonstrates a peak for the intermediate h as shown in Fig. 3. We observe that the peak value of ΔS increases with N , which may diverge at the transition point. The position of the peak h_p is smaller than the previously identified h_c and it shows a trend of approaching h_c with the increase of N . These results are consistent with the phenomenological theory⁶⁷ established based on the real

space renormalization group studies, which indicate that we are observing intrinsic properties of the MBL phase and the related quantum phase transition for system sizes we study.

B. Mobility edge and mobility gap

We have shown that the disorder can drive a quantum phase transition, where all states near the center of energy spectrum are localized. In fact, all other states with different energy density are also localized, thus we enter the full MBL phase tuned by h (see Fig. 4(c) as an example). To address the issue if the mobility edge naturally exists in such a system separating low energy states with the area-law entanglement entropy from higher energy states with volume-law behavior, we follow lower energy eigenstate by obtaining hundreds of these eigenstates in ED. We follow the entropy of each energy eigenstate S_i in the lower energy density regime and average that over 1000 disorder configurations.

As shown in Fig. 4(a-b) for $h = 2$ and 4, we identify that the disorder configuration averaged entropy S_i for the $i - th$ energy eigenstate is a smooth increasing function of eigen energy E_i or its average energy density $\varepsilon_i = \langle (E_i - E_0)/(E_{max} - E_0) \rangle$. The entropy per site S_i/N for different system sizes $N = 6 \times 2, 8 \times 2$ and 10×2 crosses around a critical energy density ε_c , which separates higher energy states with volume-law entropy (delocalized states) from lower energy localized states with S_i/N approaching zero violating the volume law. Here all the data we show have even $N_x = 6, 8$ and 10 with reduced finite size effect. The crossing point determines the mobility edge. With increasing h , the entropy of the low-lying eigenstate is reduced and the mobility edge is being pushed to the higher energy density from

$\varepsilon_c \sim 0.075$ at $h = 2$ to $\varepsilon_c \sim 0.1$ at $h = 4$. As shown in Fig. 4(c), we further move to the stronger disorder case, at $h = 10$, we see that S/N at different energy density (here we averaged over both disorder configurations and energy eigenstates for each energy density ε) is always a decreasing function with increasing N demonstrating all states are localized.

IV. SUMMARY AND DISCUSSION

We have identified the disorder driven dynamic quantum phase transition from ergodic delocalized phase to an MBL non-ergodic phase for two-leg ladder Heisenberg spin systems with random field disorder. The characteristic distributions of the entanglement entropy for both the delocalized Griffiths phase and the MBL phase agree with the theoretical description for the MBL⁶⁷. Furthermore, we show that for weaker h , energy eigenstates with higher energy density are delocalized, while states at lower density are localized, which defines a mobility edge separating these two dynamically distinct quantum states in agreement with earlier results for 1D spin chain systems^{26,46}. On the quantitative side, we find that the Heisenberg ladder requires a much higher critical disorder strength compared to the 1D spin chain model⁴⁶ to enter the full MBL phase. It is highly desired to further study multi-leg ladders and explore scaling behaviors to the 2D limit, which we leave for a future study.

Acknowledgments - We thank Tarun Grover and David Huse for stimulating discussions. This work is supported by US National Science Foundation Grants PREM DMR-1205734 (EB), DMR-1408560, and Princeton MRSEC Grant DMR-1420541 for travel support.

-
- ¹ P. W. Anderson, Phys. Rev. **109**, 1492 (1958).
² D. M. Basko, I. L. Aleiner, and B. L. Altshuler, Annals of Physics **321**, 1126 (2006).
³ L. Fleishman and P. W. Anderson, Phys. Rev. B **21**, 2366 (1980).
⁴ B. L. Altshuler, Y. Gefen, A. Kamenev, and L. S. Levitov, Phys. Rev. Lett. **78**, 2803 (1997).
⁵ P. Jacquod and D. L. Shepelyansky, Phys. Rev. Lett. **79**, 1837 (1997).
⁶ B. Georgeot and D. L. Shepelyansky, Phys. Rev. Lett. **81**, 5129 (1998).
⁷ I. V. Gornyi, A. D. Mirlin, and D. G. Polyakov, Phys. Rev. Lett. **95**, 206603 (2005).
⁸ R. Nandkishore and D. A. Huse, Annu. Rev. Cond. Matt. Phys. **6**, 15 (2015).
⁹ E. Altman and R. Vosk, Annu. Rev. Cond. Matt. Phys. **6**, 383 (2015).
¹⁰ R. Nandkishore, S. Gopalakrishnan, and D. A. Huse, Phys. Rev. B **90**, 064203 (2014).
¹¹ M. Rigol, V. Dunjko, and M. Olshanii, Nature (London) **452**, 854 (2008).
¹² M. Serbyn, M. Knap, S. Gopalakrishnan, Z. Papić, N. Y. Yao, C. R. Laumann, D. A. Abanin, M. D. Lukin, and E. A. Demler, Phys. Rev. Lett. **113**, 147204 (2014).
¹³ M. P. Kwasirogroch and N. R. Cooper, Phys. Rev. A **90**, 021605 (2014).
¹⁴ D. A. Huse, R. Nandkishore, and V. Oganesyan, Phys. Rev. B **90**, 174202 (2014).
¹⁵ M. Serbyn, Z. Papić, and D. A. Abanin, Phys. Rev. Lett. **111**, 127201 (2013).
¹⁶ A. Chandran, V. Khemani, C. R. Laumann, and S. L. Sondhi, Phys. Rev. B **89**, 144201 (2014).
¹⁷ T. Grover, ArXiv e-prints (2014), 1405.1471.
¹⁸ N. Y. Yao, C. R. Laumann, S. Gopalakrishnan, M. Knap, M. Müller, E. A. Demler, and M. D. Lukin, Phys. Rev. Lett. **113**, 243002 (2014).
¹⁹ R. Vasseur, S. A. Parameswaran, and J. E. Moore, Phys. Rev. B **91**, 140202 (2015).
²⁰ V. Ros, M. Müller, and A. Scardicchio, Nucl. Phys. B **891**, 420 (2015).
²¹ V. Oganesyan and D. A. Huse, Phys. Rev. B **75**, 155111 (2007).
²² A. Pal and D. A. Huse, Phys. Rev. B **82**, 174411 (2010).
²³ M. Žnidarič, T. Prosen, and P. Prelovšek, Phys. Rev. B **77**, 064426 (2008).
²⁴ E. Canovi, D. Rossini, R. Fazio, G. E. Santoro, and A. Silva, Phys. Rev. B **83**, 094431 (2011).
²⁵ E. Cuevas, M. Feigel'Man, L. Ioffe, and M. Mezard, Nat. Com-

- mun. **3**, 1128 (2012).
- ²⁶ J. A. Kjäll, J. H. Bardarson, and F. Pollmann, Phys. Rev. Lett. **113**, 107204 (2014).
- ²⁷ A. De Luca and A. Scardicchio, EPL (Europhysics Letters) **101**, 37003 (2013).
- ²⁸ S. Iyer, V. Oganesyan, G. Refael, and D. A. Huse, Phys. Rev. B **87**, 134202 (2013).
- ²⁹ S. Johri, R. Nandkishore, and R. N. Bhatt, ArXiv e-prints (2014), 1405.5515.
- ³⁰ J. H. Bardarson, F. Pollmann, and J. E. Moore, Phys. Rev. Lett. **109**, 017202 (2012).
- ³¹ F. Andraschko, T. Enss, and J. Sirker, Phys. Rev. Lett. **113**, 217201 (2014).
- ³² C. R. Laumann, A. Pal, and A. Scardicchio, Phys. Rev. Lett. **113**, 200405 (2014).
- ³³ J. M. Hickey, S. Genway, and J. P. Garrahan, ArXiv e-prints (2014), 1405.5780.
- ³⁴ A. Nanduri, H. Kim, and D. A. Huse, Phys. Rev. B **90**, 064201 (2014).
- ³⁵ Y. Bar Lev and D. R. Reichman, Phys. Rev. B **89**, 220201 (2014).
- ³⁶ B. Bauer and C. Nayak, J. Stat. Mech. Theor. Exp. **9**, 09005 (2013).
- ³⁷ J. Z. Imbrie, ArXiv e-prints (2014), 1403.7837.
- ³⁸ M. Serbyn and J. E. Moore, ArXiv e-prints (2015), 1508.07293.
- ³⁹ R. Singh, J. H. Bardarson, and F. Pollmann, ArXiv e-prints (2015), 1508.05045.
- ⁴⁰ Y. Bar Lev and D. R. Reichman, ArXiv e-prints (2015), 1508.05391.
- ⁴¹ D.-L. Deng, J. H. Pixley, X. Li, and S. Das Sarma, ArXiv e-prints (2015), 1508.01270.
- ⁴² X. Chen, X. Yu, G. Y. Cho, B. K. Clark, and E. Fradkin, ArXiv e-prints (2015), 1509.03890.
- ⁴³ D. Pekker, G. Refael, E. Altman, E. Demler, and V. Oganesyan, Phys. Rev. X **4**, 011052 (2014).
- ⁴⁴ Y. Huang, ArXiv e-prints (2015), 1507.01304.
- ⁴⁵ Y.-Z. You, X.-L. Qi, and C. Xu, ArXiv e-prints (2015), 1508.03635.
- ⁴⁶ D. J. Luitz, N. Laflorencie, and F. Alet, Phys. Rev. B **91**, 081103 (2015).
- ⁴⁷ A. C. Potter, R. Vasseur, and S. A. Parameswaran, ArXiv e-prints (2015), 1501.03501.
- ⁴⁸ J. M. Deutsch, Phys. Rev. A **43**, 2046 (1991).
- ⁴⁹ M. Srednicki, Phys. Rev. E **50**, 888 (1994).
- ⁵⁰ P. Hosur and X.-L. Qi, ArXiv e-prints (2015), 1507.04003.
- ⁵¹ D. A. Huse, R. Nandkishore, V. Oganesyan, A. Pal, and S. L. Sondhi, Phys. Rev. B **88**, 014206 (2013).
- ⁵² Y. Bahri, R. Vosk, E. Altman, and A. Vishwanath, ArXiv e-prints (2013).
- ⁵³ R. Vosk and E. Altman, Phys. Rev. Lett. **112**, 217204 (2014).
- ⁵⁴ A. C. Potter and A. Vishwanath, ArXiv e-prints (2015), 1506.00592.
- ⁵⁵ N. Y. Yao, C. R. Laumann, and A. Vishwanath, ArXiv e-prints (2015), 1508.06995.
- ⁵⁶ A. Chandran, J. Carrasquilla, I. H. Kim, D. A. Abanin, and G. Vidal, Phys. Rev. B **92**, 024201 (2015).
- ⁵⁷ P. Ponte, Z. Papić, F. Huveneers, and D. A. Abanin, Phys. Rev. Lett. **114**, 140401 (2015).
- ⁵⁸ T. Grover and M. P. A. Fisher, J. Stat. Mech. Theor. Exp. **10**, 10010 (2014).
- ⁵⁹ D. Pekker and B. K. Clark, ArXiv e-prints (2014), 1410.2224.
- ⁶⁰ V. Khemani, F. Pollmann, and S. L. Sondhi, ArXiv e-prints (2015), 1509.00483.
- ⁶¹ X. Yu, D. Pekker, and B. K. Clark, ArXiv e-prints (2015), 1509.01244.
- ⁶² D. Pekker and B. K. Clark, ArXiv e-prints (2014), 1410.2224.
- ⁶³ M. Friesdorf, A. H. Werner, W. Brown, V. B. Scholz, and J. Eisert, Phys. Rev. Lett. **114**, 170505 (2015).
- ⁶⁴ F. Pollmann, V. Khemani, J. I. Cirac, and S. L. Sondhi, ArXiv e-prints (2015), 1506.07179.
- ⁶⁵ A. Chandran, I. H. Kim, G. Vidal, and D. A. Abanin, Phys. Rev. B **91**, 085425 (2015).
- ⁶⁶ T. Devakul and R. R. P. Singh, ArXiv e-prints (2015), 1508.04813.
- ⁶⁷ R. Vosk, D. A. Huse, and E. Altman, ArXiv e-prints (2014), 1412.3117.
- ⁶⁸ W. de Roeck, F. Huveneers, M. Müller, and M. Schiulaz, ArXiv e-prints (2015), 1506.01505.
- ⁶⁹ I. Mondragon-Shem, A. Pal, T. L. Hughes, and C. R. Laumann, ArXiv e-prints (2015), 1501.03824.
- ⁷⁰ X. Wan, D. N. Sheng, E. H. Rezayi, K. Yang, R. N. Bhatt, and F. D. M. Haldane, Phys. Rev. B **72**, 075325 (2005).
- ⁷¹ D. N. Sheng, X. Wan, E. H. Rezayi, K. Yang, R. N. Bhatt, and F. D. M. Haldane, Phys. Rev. Lett. **90**, 256802 (2003).
- ⁷² L. Sheng, D. N. Sheng, F. D. M. Haldane, and L. Balents, Phys. Rev. Lett. **99**, 196802 (2007).
- ⁷³ Y. Y. Atas, E. Bogomolny, O. Giraud, and G. Roux, Phys. Rev. Lett. **110**, 084101 (2013).
- ⁷⁴ M. L. Mehta, *Random matrices* (Academic Press, Boston, New York, San Diego, 1991), ISBN 0-12-488051-7.
- ⁷⁵ H. F. Song, S. Rachel, C. Flindt, I. Klich, N. Laflorencie, and K. Le Hur, Phys. Rev. B **85**, 035409 (2012).